Strain engineering water transport in graphene nanochannels

Wei Xiong,[1] Jefferson Zhe Liu,[2,*] Ming Ma,[1] Zhiping Xu,[1] John Sheridan,[2] and Quanshui Zheng[1,3,†]

[1]*Department of Engineering Mechanics and Center for Nano and Micro Mechanics, Tsinghua University, Beijing 100084, China*
[2]*Department of Mechanical and Aerospace Engineering, Monash University, Clayton, VIC 3800, Australia*
[3]*Institute of Advanced Study, Nanchang University, Nanchang, China*

Using equilibrium and nonequilibrium molecular dynamic simulations, we found that engineering the strain on the graphene planes forming a channel can drastically change the interfacial friction of water transport through it. There is a sixfold change of interfacial friction stress when the strain changes from -10% to 10%. Stretching the graphene walls increases the interfacial shear stress, while compressing the graphene walls reduces it. Detailed analysis of the molecular structure reveals the essential roles of the interfacial potential energy barrier and the structural commensurateness between the solid walls and the first water layer. Our results suggest that the strain engineering is an effective way of controlling the water transport inside nanochannels. The resulting quantitative relations between shear stress and slip velocity and the understanding of the molecular mechanisms will be invaluable in designing graphene nanochannel devices.

I. INTRODUCTION

Graphene, due to its extremely large specific surface area [1] and superior electronic and mechanical properties, is a promising material in energy storage, catalysis, and novel nanofluidic device applications such as super-capacitors, photocatalysis, water desalination, nanofiltration, etc. [1–5]. In practice, graphene layers usually self-assemble in paperlike structures with interlayer distance on the nanometer scale [6,7]. Fluid transport in such flat nanochannels is a key concern in improving the performance and the efficiency of the devices. Water confined inside nanochannels exhibits a large slippage. Experiments have shown that the flow rate of water inside carbon nanotubes (CNTs) is several orders of magnitude higher than predicted by conventional hydrodynamics [8–10]. Because of their structural similarity, the extremely fast water transport found inside CNTs is also expected in graphene nanochannels. A deep understanding of the molecular transport and the means of controlling the water transport inside graphene flat nanochannels is highly desired in practice.

The structural properties of the single atomic layer of graphene, to a large extent, are determined by its interactions with the environment. For example, an epitaxial strain on the order of $\pm 1\%$ builds up in the graphene when it is grown on different substrates [11–14]; electromechanical strain on the order of ± 1–2 % results from charge injection in the graphene [15]; and applying mechanical force (e.g., nanoindentation) on the graphene can lead to a strain of about 10% [16]. Meanwhile, due to the size confinement in the CNT and graphene nanochannels, the first water layer next to the solid walls tends to be ordered [17]. It is reasonable to expect that the slip flow of water over the graphene layers will be analogous to the friction between two ordered crystal planes, meaning the interfacial commensurateness will play an essential role. Strain engineering of graphene layers to alter the

interfacial molecular structures could thus provide a method of controlling the flow in nanofluidic devices.

Here, we use both equilibrium and nonequilibrium MD simulations to study the water flowing in uniformly biaxial strained graphene nanochannels. The relations between the interfacial friction shear stress τ and the slip velocity v_s are obtained. Our results show that the interfacial friction coefficient (i.e., ratio of τ over v_s) increases almost sixfold when the strains applied to graphenes vary from -10% to 10%. To gain a deep understanding of the physics behind this remarkable change, the molecular mechanisms, such as the interfacial potential barrier, density, and structure factor of the first water layer, are quantitatively investigated.

II. SIMULATION DETAILS

Both equilibrium and nonequilibrium molecular dynamic (MD) simulations were performed. Our molecular system is illustrated in Fig. 1(a): water flows between two graphene sheets with an interlayer distance of about 2 nm. Uniform in-plane biaxial strain $\epsilon = (a_{CC} - a_{CC_0})/a_{CC_0}$ is applied ranging from -10% up to 10% to the graphene walls, where a_{CC} and $a_{CC_0} = 0.142$ nm denote the carbon-carbon bond length of the strained and strain-free graphene, respectively. Accordingly the a_{CC} changes from $0.9a_{CC_0}$ to $1.1a_{CC_0}$. To ensure the internal pressure of water at 1 atm, we fix one of the graphene walls and use the other one as a piston to impose the pressure at a given temperature (300 K). The positions of carbon atoms are then fixed in the following MD simulations. We noticed that fixing solid walls in highly confined fluid could lead to unphysical material properties and underlying dynamics [18]. So we simulated the flow in a zero-strained channel with flexible graphene walls and found the difference of the friction shear stress is $<10\%$ in comparison to the fixed wall case. Periodic boundary conditions are applied along the two directions in the plane. Along the flow direction [x direction in Fig. 1(a)], the simulation box length was chosen to be 6.0 nm. However, we also performed simulations with a longer length of 20 nm for the zero-strain case and found the differences in the calculated
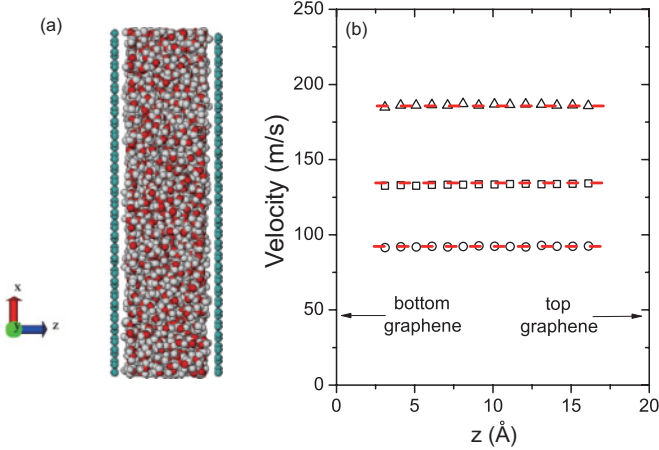
*zhe.liu@monash.edu
†zhengqs@tsinghua.edu.cn

FIG. 1. (Color online) (a) Water flow inside a graphene flat nanochannel with a height of ∼2 nm. (b) The pluglike velocity profile of the Poiseuille flow along the flow direction (i.e., x direction) observed in our MD simulations. We applied three different accelerations to water molecules to obtain the different steady flow velocities as shown by the different symbols.

friction stress were negligible. There are 1200–2000 water molecules in our systems.

All MD simulations were performed with the LAMMPS code [19]. A time step of 1.0 fs was used and the total simulation time was about a few nanoseconds. We used the CHARMM force field and the SPC/E model [20] for water with the SHAKE algorithm [21]. The water-carbon interactions were described by a Lennard-Jones (LJ) potential between oxygen and carbon atoms with parameters $\epsilon = 4.063$ meV and $\sigma = 0.3190$ nm, yielding a contact angle of 95º between the water and strain-free graphene [22]. The van der Waals forces were truncated at 1.2 nm with long-range Columbic interactions computed using the particle-particle particle-mesh (PPPM) algorithm [23]. Water molecules were kept at a constant temperature of 300 K using the Berendsen thermostat, with the temperature calculated after removing the center-of-mass velocity. Recent studies show that thermostatting could have a significant effect in the dynamics of a strongly driven confined fluid [18]. So we also tried the Nosé-Hoover thermostat applied to the degrees of freedom perpendicular to the flow direction in the zero-strain case. No significant differences between these two thermostats were found in our study.

In our nonequilibrium MD simulations (NEMD), the Poiseuille flow was driven by applying a constant gravitylike acceleration to all the oxygen and hydrogen atoms. Different external accelerations were applied to achieve a set of steady flows of different velocity (once the external forces were balanced by the friction). It usually took a few hundred picoseconds to reach a steady flow and the simulations were then continued for five more nanoseconds to collect data. By applying different accelerations from 0 to 0.004 nm/ps^2, we obtained the steady-flow velocities from 0 to 200 m/s. Velocity profiles of the Poiseuille flows in our nanochannels are pluglike as shown in Fig. 1(b), so we can set the slip velocity equal to the average velocity. We noted that a similar simplification was adopted in Ref. [24]. The friction shear stress was calculated from the external force as $\tau = Nma/2A$,
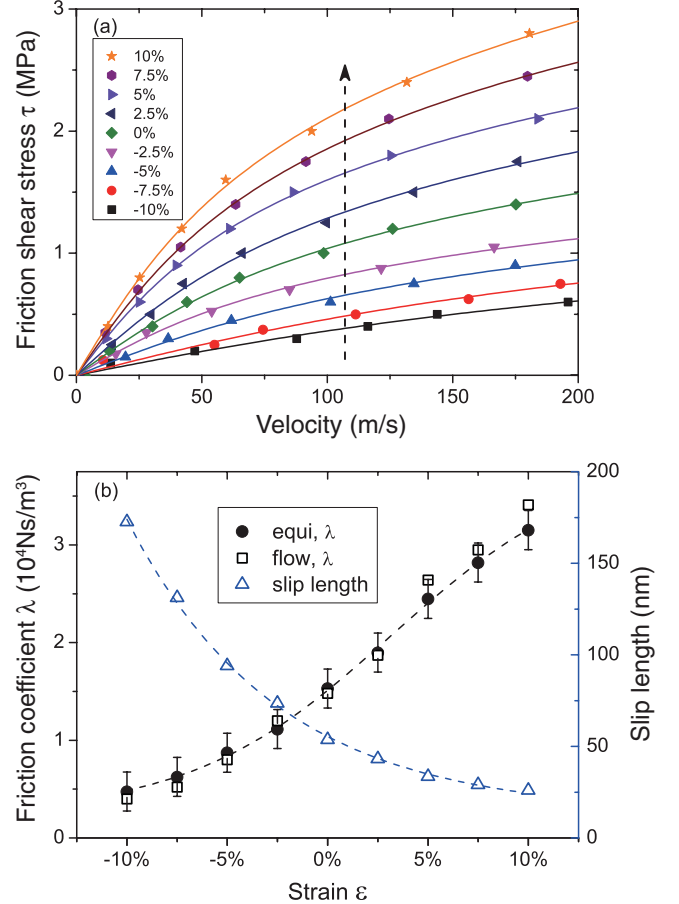

FIG. 2. (Color online) (a) Friction shear stress τ versus slip velocity v_s at the water/graphene interface with graphene deformation strain ϵ from −10% to 10% (indicated by the arrow from bottom to top). The solid lines represent the fitted relations $\tau/\tau_0 = \mathrm{asinh}(v_s/v_0)$, with the fitting coefficients τ_0 and v_0 summarized in Table I. (b) The friction coefficient λ and the slip length l_s as a function of the applied strain ϵ. The open square symbols represent the λ values calculated from the slopes of curves at $v_s = 0.0$ in (a), and the solid circles are calculated by using the Green-Kubo (GK) relation [Eq. (2)] in our equilibrium MD simulations. The slip length l_s is calculated by using $l_s = \mu/\lambda$ [26], where μ is the viscosity of water.

where N is the number of water molecules, m is the mass of one water molecule, a is the acceleration, and A is the area of one graphene sheet. For comparison, we also calculated the shear stress τ using the forces in the flow direction acting on carbon atoms (due to pairwise interactions between the carbon atoms and the water molecules) and found good agreement, e.g., the difference is <5%.

III. RESULTS AND DISCUSSIONS

A. Strain dependent friction coefficient from MD simulations

Figure 2(a) shows the interfacial friction shear stress τ as a function of flow velocity v_s in the graphene channels placed under different strain. They are fitted well using an inverse hyperbolic sine (IHS) relationship $\tau/\tau_0 = \mathrm{asinh}(v_s/v_0)$. The values of τ_0 and v_0 derived from the fits are summarized in Table I for different strain values. The IHS relation's derivation arises from the transition state theory model of Yang [25],

TABLE I. Fitted parameters τ_0 and v_0 in the inverse hyperbolic-sine relationship, $\tau/\tau_0 = \mathrm{asinh}(v_s/v_0)$, which describes the water slip flow in the strained graphene nanochannels. The friction coefficient λ and slip length l_s are also calculated (see text for details).

ϵ	−10%	−7.5%	−5.0%	−2.5%	0%	2.5%	5.0%	7.5%	10%
τ_0 (MPa)	0.457	0.528	0.507	0.487	0.688	0.827	0.880	1.059	1.183
v_0 (m/s)	113.6	101.5	63.4	40.7	46.5	44.2	33.4	35.8	34.7
$\lambda = \tau_0/v_0$ (10^4 N s/m^3)	0.40	0.52	0.80	1.20	1.48	1.87	2.64	2.96	3.41
$l_s = \mu/\lambda$ (nm)	173	131	94	74	54	43	34	29	26

in which the slip flow is described as a collective thermal diffusion of fluid atoms over a periodic solid wall. We have previously justified the use of this relation by using large-scale NEMD simulations for water flowing inside CNTs [24]. Figure 2(a) shows that the friction shear stress increases with an increase of strain.

At low flow rates (e.g., $v_s < 10$ m/s), the IHS relationship exhibits a linear relation $\tau \cong \lambda v_s$, where the friction coefficient λ is often used to represent the strength of friction. Intrinsically, the friction coefficient is the physically relevant property to characterize the interfacial dynamics [26]. The open squares in Fig. 2(b) depict the friction coefficients λ [slopes of the τ-v_s curves at $v_s = 0.0$ in Fig. 2(a)] as a function of the applied strain ϵ. The key result of Fig. 2 is the dramatic effect of the strain on the friction shear stress and the friction coefficient. Stretching the graphene layer leads to the increase of the friction stress with a twofold increase of the friction coefficient at the 10% strain. Compressing the graphene layer results in a significant reduction in the friction coefficient, e.g., about threefold at the −10% strain. In the strain-free state, our calculated friction coefficient is close to the value from Falk *et al.*, 1.48 vs 1.20 (10^4 Ns/m^3) [27]. The difference can be attributed to the different water models and the different LJ potential parameters used to describe the carbon-oxygen interactions (possibly yielding different contact angles). Compared to our previous MD simulations of water transport inside a double-walled CNT with a diameter of 2 nm [24], the friction coefficient of the graphene channel is higher, i.e., 1.48 vs 0.3 (10^4 Ns/m^3), which is consistent with the conclusion of Falk *et al.* [27] that λ depends on the degree of curvature.

Since the slip length is a widely used quantity to describe the slip flow, we converted our friction coefficients λ to the slip lengths l_s by using $l_s = \mu/\lambda$ [26], where μ is the viscosity of water (0.82 mPa s for the SPC/E water model at 300 K [28]). The results are plotted in Fig. 2(b). At the strain-free state (i.e., $\epsilon = 0$), the slip length l_s is about 54 nm. Such a large slip length in comparison to the channel height of 2 nm implies the pluglike speed profile shown in Fig. 1(b). We note that although our calculated slip length is significantly higher than the value obtained by Thomas *et al.*, ~ 30 nm [29], the qualitative form of the agreement is reasonable. We believe that the discrepancy arises from the different water model (TIP5P) adopted. Overall, however, the remarkable effect shown in these results is the degree to which strain engineering of the graphene planes can significantly change the slip length from 26 nm up to 173 nm.

The sensitive dependence of the friction coefficient λ and the slip length l_s on the strain (Fig. 2) suggests that the strain engineering indeed can serve as an effective method of controlling the water transport inside the graphene nanochannels. It may also be an important factor in our better understanding of why there is such scatter in experimental and numerical results for slip lengths of water transport inside the CNTs; this can range from several nanometers up to several micrometers [8–10,30,31]. To gain a deep physical insight into how the molecular mechanisms affect the drastic changes arising from the imposed strain, we investigated the phenomenon further; the results of that research is provided in the following sections.

B. Molecular structures of water inside a graphene nanochannel

It is known that the interfacial molecular structures determine the slip flow over a hydrophobic surface. In this section, we study the structural details of our water/graphene-channel system.

Density profiles of the water molecules across the height of the graphene channels are shown in Fig. 3(a). In the strain-free graphene channel, our MD results found almost no difference between the densities of the water molecules at rest and at a flow rate of 100 m/s. The sharp peak indicates the position of the first liquid layer, i.e., 3.25 Å, from the solid walls. When different strains (−10% and 10%) are imposed on the graphene planes there is no change in the locations of the first density peaks, whereas the peak heights do decrease with the strain. The inset of Fig. 3(a) summarizes the density change with respect to the strains. We believe that the reason for the density drop is the weakened attraction between the solid walls and the water molecules, arising from the low surface density of the carbon atoms caused by the stretching of the graphene layer.

The two-dimensional radial density function (RDF) of the first liquid layer was also calculated. By normalizing the RDF with the mean density, we found that the RDFs almost overlap with each other for the differently strained graphene channels, as indicated in Fig. 3(b) at strains of −10%, 0%, and 10%. This implies that strain engineering on the solid walls has a negligible effect on the structures of the first water layer. In comparison, the RDF of the bulk water is shown as the dashed line in Fig. 3(b). The fact that the first peak is in almost the same position in this case suggests that the average oxygen-oxygen interatomic distance of the neighbored water molecules is unaffected in the graphene nanochannels, i.e., $r_{OO} = 0.275$ nm. We can thus conclude that the size confinement actually leads to more compact water molecules in the first liquid layer than in the bulk water without changing the intermolecular distance.
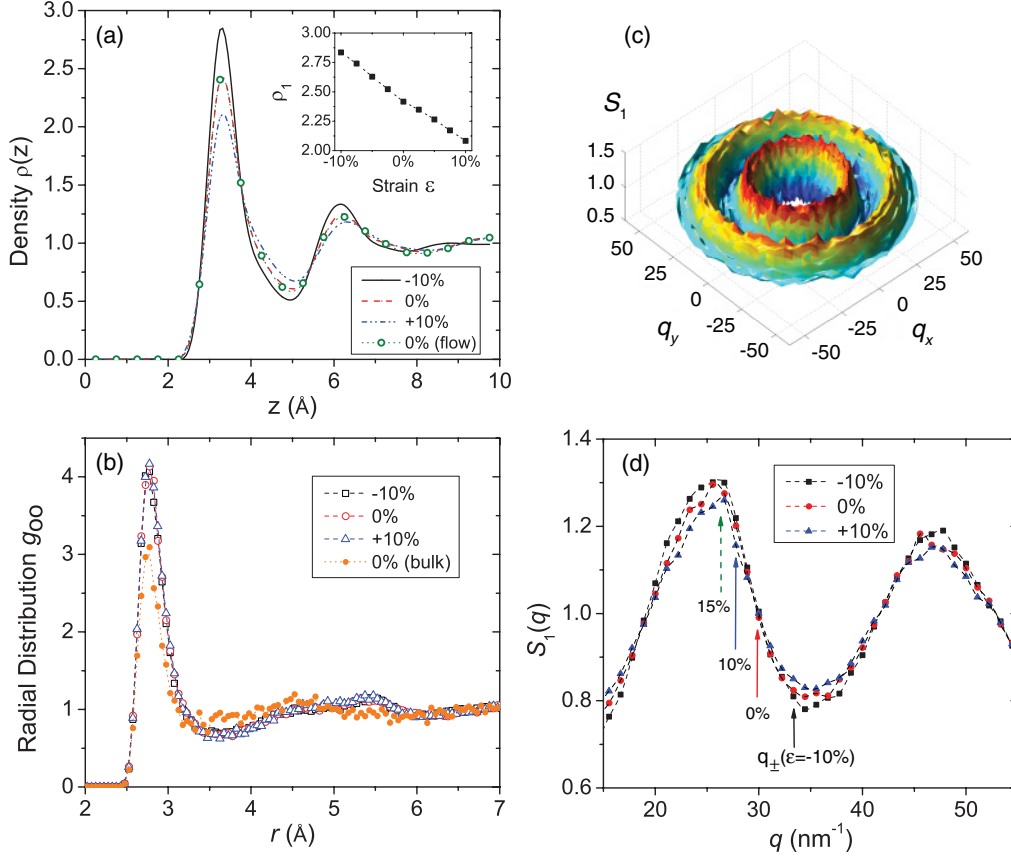
FIG. 3. (Color online) (a) Density profiles of water across the height (z direction) of the graphene nanochannel. The sharp density peak next to the solid wall represents the first water layer. For graphene layers at zero strain, the density profiles at flow velocity $v_s = 0$ m/s and $v_s = 100$ m/s have a negligible difference. The density profiles in the strained graphene channels with $\epsilon = -10\%$ (solid line), 0% (dashed line), and 10% (dash-dotted line) indicate the almost same first peak position but different magnitude. The inset shows the density of the first peak as a function of the imposed strains ϵ on graphene. (b) Two-dimensional radial density function (RDF, normalized by the mean density) of the first water layer in three differently strained graphene channels, $\epsilon = -10\%$ (open square), 0% (open circle), and 10% (open triangle). In comparison, the RDF of the bulk water is also shown. (c) Two-dimensional structure factor $S_1(\mathbf{q})$ of the first water layer in the strain-free graphene channel exhibits a clear direction independence. (d) The radial average of the structure factor in the strained graphene channels with $\epsilon = -10\%$ (solid square), 0% (solid circle), and 10% (solid triangle). The solid arrows indicate the positions of the reciprocal lattice vector $|q_\pm|$ of the strained graphene planes.

The two-dimensional structure factor of the first water layer was calculated by using the following expression [27,32]:

$$S_1(\mathbf{q}) = \left\langle \frac{1}{N} \sum_{j=1}^{N} \sum_{l=1}^{N} e^{i\mathbf{q}\cdot(\mathbf{r}_l - \mathbf{r}_j)} \right\rangle$$
$$= \left\langle \frac{1}{N} \left[\left(\sum_{j=1}^{N} \cos(\mathbf{q}\cdot\mathbf{r}_j) \right)^2 + \left(\sum_{j=1}^{N} \sin(\mathbf{q}\cdot\mathbf{r}_j) \right)^2 \right] \right\rangle,$$

(1)

where $\mathbf{r}_j$ represents the position of the jth oxygen atom, N is the number of oxygen atoms in the first water layer, and $\mathbf{q}$ is the two-dimensional reciprocal lattice vector. The brackets $\langle \rangle$ denote an equilibrium ensemble average. Figure 3(c) shows the structure factor of water inside the zero-strained graphene channel. It is clear that the structure factor is almost independent of the direction of the $\mathbf{q}$ vector. Similar isotropic structure factors are also observed in the strained graphene channels. We then averaged the $S_1(\mathbf{q})$ along all the $\mathbf{q}$ directions

and plot the $S_1(q)$ in Fig. 3(d) with $q = |\mathbf{q}|$ representing the length of the reciprocal lattice vector. The very small differences in the plots of $S_1(q)$ confirm our conclusion that the strain engineering on graphene walls does not affect the structures of the first water layer. However, the strain engineering does change the interfacial commensurateness due to the change of the graphene. The solid arrows in Fig. 3(d) represent the positions of the reciprocal lattice vectors of the differently strained graphene planes $|\mathbf{q}_\pm|$. Here the lattice vectors of graphene are connecting the centers of two six-rings in neighbors. With the strains from -10% to 10%, it is evident that $S_1(|\mathbf{q}_\pm|)$ increases, which suggests a better degree of commensurateness.

The inset of Fig. 4 shows the interfacial potential energy profile over a graphene ($\epsilon = 0$) at the position of the first water layer, i.e., $z_1 = 3.25$ Å indicated in Fig. 3(a). The energy profile has a sixfold symmetry. In our analysis, the energy barrier $\Delta E(z_1)$ is defined as the difference of the potential energy between the maximum points (located on top of the carbon atoms) and the minimum points (located in the center
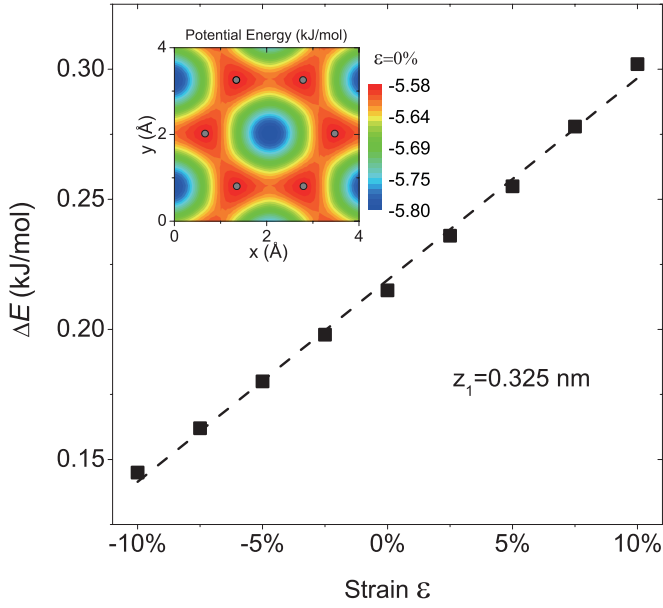
FIG. 4. (Color online) Interfacial potential energy barriers as a function of the strain applied on the graphene walls. The contour plot of potential energy landscape at $\epsilon = 0$ is shown in inset with a sixfold symmetry, which is consistent to the atomic structure of graphene.

of the six-rings). Figure 4 depicts a linear relation of the calculated energy barrier $\Delta E(z_1)$ with respect to the exerted strain. The magnitude of the energy barrier doubles when the strain ϵ changes from -10% to 10%.

C. A microscopic understanding on strain dependent friction

As a dissipation coefficient, the friction coefficient λ can be expressed via the Green-Kubo (GK) relationship, which relates λ to the autocorrelation function of fluctuating pairwise forces at equilibrium [33]

$$\lambda = \frac{1}{A k_B T} \int_0^\infty \langle \mathbf{F}(t)\mathbf{F}(0)\rangle dt, \quad (2)$$

where $\mathbf{F}(t)$ is the total forces in the flow direction exerted on carbon atoms due to the interactions with water molecules in our equilibrium MD simulations, k_B is the Boltzmann constant, A is the surface area, and T is the water temperature. We directly calculated the force autocorrelation function $\langle \mathbf{F}(t)\mathbf{F}(0)\rangle$ in our equilibrium MD simulations with a simulation time of 5 ns. Here, we should point out that a well-documented difficulty of estimating the GK relationships via the equilibrium MD is the finite size of the simulated system, which often leads to a vanishing of the friction coefficient after a very long time simulation [33,34]. The integration should thus have a cutoff time t_0. A widely adopted method of resolving this is to use the onset of a plateau of the integrations as the cutoff t_0. In our simulations, however, it was difficult to locate the plateau in some cases. So we followed the suggestions from Refs. [34,35] and chose t_0 as the first zero of the force autocorrelation function; typically this was in the range [1 ps, 10 ps]. The friction coefficients calculated from our equilibrium MD simulations [Eq. (2)] are shown as the solid circles in Fig. 2(b). A good agreement can be observed
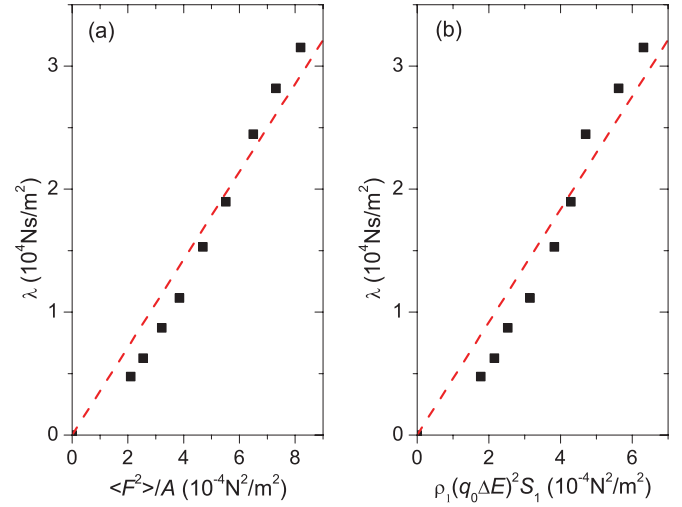

FIG. 5. (Color online) (a) Functional dependence of the friction coefficient λ versus the static root mean square force $\langle F^2 \rangle$ [Eq. (3)]. (b) Functional dependence of the friction coefficient λ on the computed $\rho_1(q_0\Delta E)^2 S_1$ [Eq. (4)]. Dashed straight lines are guides to the eye. The good linear relations validate the forms of Eqs. (3) and (4).

in comparison with the NEMD results, which suggests the GK relation is applicable in our systems. It is worth noting that some recent studies conclude that the viscous friction coefficient calculated by Eq. (2) depends on the size of the system [36,37]. In our MD simulations, however, the plug flow suggests that the viscosity should have a small effect on the slippage at the interface. We believe the size of the molecular system does not affect our results.

To gain further insight of the molecular mechanisms, we consider the GK expression [Eq. (2)] in more detail. The GK relation can be reexpressed as [27]

$$\lambda = \frac{\tau_F}{A k_B T} \langle \mathbf{F}^2 \rangle. \quad (3)$$

In our equilibrium MD simulations, we find that the decorrelation time $\tau_F = \int \langle \mathbf{F}(t)\mathbf{F}(0)\rangle / \langle \mathbf{F}^2 \rangle$, weakly depends on the exerted strains on the graphenes. Typically it is 100–160 fs for $-10\% \leqslant \epsilon \leqslant 10\%$, which is consistent with the MD results of water flow in CNTs [27]. Since the variance of τ_F (60%) is one order of magnitude smaller than that of λ (600%), the main contribution to the variance of λ must be from the static rms force $\langle \mathbf{F}^2 \rangle$. In other words, the change of the friction coefficients λ with respect to the strains should be directly correlated with $\langle \mathbf{F}^2 \rangle$. Indeed, as shown in Fig. 5(a), the good linear relation between λ and $\langle \mathbf{F}^2 \rangle/A$ suggests that the decorrelation time τ_F can be approximated as a constant.

Following Ref. [27], the rms force $\langle \mathbf{F}^2 \rangle$ can be estimated analytically. If we assume the main contribution of the friction shear stress arises from the first liquid layer, one can approximate the total rms force as

$$\frac{\langle \mathbf{F}^2 \rangle}{A} \cong \frac{1}{2}\rho_1 [S_1(\mathbf{q}_+) + S_1(\mathbf{q}_-)] (q_0\Delta E)^2, \quad (4)$$

where ρ_1 is the density of the first water layer, S_1 is the two-dimensinonal structure factor of the first water layer,
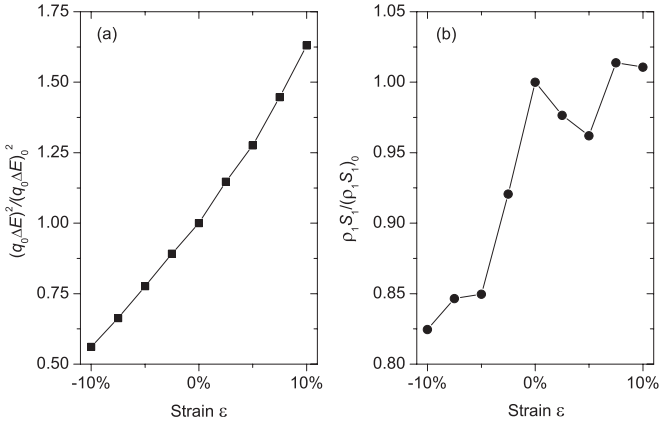
FIG. 6. (a) The normalized energy barrier of the potential profiles from the graphene solid walls as a function of the strains applied. (b) The normalized structural changes as the function of the applied strains on the solid walls.

and $\Delta E = \Delta E(z_1)$ is the energy barrier. The reciprocal lattice vector of the graphene wall is $\mathbf{q}_\pm = q_0(1/\sqrt{3}; \pm 1)$ with $q_0 = 2\pi/(\sqrt{3}a_{CC})$ and a_{CC} the carbon-carbon bond length. Figure 5(b) shows the comparison of the friction coefficients directly calculated from our MD simulations [Fig. 2(b)] and those computed by using the analytical expressions in Eq. (4). The good linear relation clearly validates the form of Eq. (4). This is an important result because we can quantitatively analyze the effects of density ρ_1, structure factor $S_1(\mathbf{q}_\pm)$, and energy barrier ΔE on the friction coefficients.

To quantify the contributions of the energy barrier and the interfacial structures to the friction coefficient λ, we normalize λ by the friction coefficient at zero strain λ_0 as $\lambda/\lambda_0 = [(q_0 \Delta E)^2/(q_0 \Delta E)_0^2][\rho_1 S_1/(\rho_1 S_1)_0]$. Figure 6 shows how each of these two terms varies as functions of the strain ϵ applied on graphene walls. When compared to Fig. 2(b), we can conclude that first, the contribution to the change of λ mainly comes from the change of the energy barrier [Fig. 6(a)]; second, in the stretched graphene nanochannels, the increase of commensurateness S_1 [Fig. 3(d)] and the reduction of the first liquid layer density ρ_1 [Fig. 3(a) inset] cancel out each other, resulting in a small overall contribution [Fig. 6(b)]; and third, when the graphene channel is under in-plane compression, the decrease of the structural factor overwhelms the increase of the density [Fig. 6(b)], meaning that, quantitatively, the contribution from $\rho_1 S_1$ is about 30% of that from ΔE toward the effect on the friction coefficient [Eq. (4)].

It is well recognized that strain engineering on graphene changes its electronic properties [38,39], which should influence the van der Waals (vdW) interactions between water molecules and graphene. To ensure the adopted LJ potential can describe the vdW interactions between water molecules and the strained graphene layer, we have carried out vdW-density functional theory (DFT) calculations by adopting Grimme's protocol [40], which has been testified for water and graphene systems recently [41]. For a single water molecule adsorbed on a strained graphene layer, we obtained good agreement on the trend of the vdW interaction energy change

as a function of the strain between the vdw-DFT and LJ potential results, i.e., stretching the graphene layer leads to weaker vdW interactions, and vice versa. It thus confirms our results on the change of the friction law or the slip length via the strain engineering (Fig. 2). It is worth noting that quantitative information regarding interactions between water molecules and graphene is still under debate in experiments [42] and in theoretical models [41]. In addition, it was observed that the water flow inside a graphene channel induced an electrical potential change in graphene along the flow direction [43,44], which could in turn affect the water flow. But the potential drop measured in experiments over one graphene unit cell length is on the order of nV [43], i.e., six orders of magnitude smaller than the energy barrier calculated in our MD simulations (Fig. 4). Thus such an induced potential has a negligible effect on our calculated flow resistance stress.

IV. CONCLUSIONS

To summarize, our MD simulations show that the friction coefficient λ (and the slip length l_s) of the water transport in the graphene nanochannels exhibits a highly sensitive dependence on the strains imposed on the graphene. The friction coefficients change by a factor of 6 when the strain on the graphene wall changes from -10% to 10%. This corresponds to a change in the slip length l_s, which varies from 173 to 26 nm. Our results suggest that strain engineering could serve as an effective route to control the water transport inside graphene nanochannels. It may also be an important factor in understanding the scatter in the reported slip lengths of the water flow inside CNTs in experiments and simulations. The molecular mechanisms of the strain effect on the slip flow are also studied. We find that the strains on the graphene have relatively small influences on the molecular structure of the first water layer, other than on the reduction of the density. Using a simplified analytical model based on the Green-Kubo relation [27], we find that the change of energy barrier makes the most important contribution to the change of the friction coefficient λ, in comparison to the effect of the water density and the structural factor (which make about 30% of the contribution made by the energy barrier). The quantitative relationship for $\tau - v_s$ provided herein when combined with the physical insights provided on the molecular mechanism will be valuable to designers of graphene nanochannels for application in nanofluidic devices.

[1] M. D. Stoller, S. Park, Y. Zhu, J. An, and R. S. Ruoff, Nano Lett. **8**, 3498 (2008).

[2] H. Li, L. Zou, L. Pan, and Z. Sun, Environ. Sci. Technol. **44**, 8692 (2010).

[3] V. Chandra, J. Park, Y. Chun, J. W. Lee, I. Hwang, and K. S. Kim, ACS Nano **4**, 3979 (2010).

[4] H. Zhang, X. Lv, Y. Li, Y. Wang, and J. Li, ACS Nano **4**, 380 (2010).

[5] J. J. Yoo, K. Balakrishnan, J. Huang, V. Meunier, B. G. Sumpter, A. Srivastava, M. Conway, A. L. M. Reddy, J. Yu, R. Vajtai, and P. M. Ajayan, Nano Lett. **11**, 1423 (2011).

[6] D. Li, M. B. Muller, S. Gilje, R. B. Kaner, and G. G. Wallace, Nat. Nanotechnol. **3**, 101 (2008).

[7] H. Chen, M. B. Mller, K. J. Gilmore, G. G. Wallace, and D. Li, Adv. Mater. **20**, 3557 (2008).

[8] M. Majumder, N. Chopra, R. Andrews, and B. J. Hinds, Nature (London) **438**, 44 (2005).

[9] J. K. Holt, H. G. Park, Y. Wang, M. Stadermann, A. B. Artyukhin, C. P. Grigoropoulos, A. Noy, and O. Bakajin, Science **312**, 1034 (2006).

[10] M. Whitby and N. Quirke, Nat. Nanotechnol. **2**, 87 (2007).

[11] K. S. Kim, Y. Zhao, H. Jang, S. Y. Lee, J. M. Kim, K. S. Kim, J.-H. Ahn, P. Kim, J.-Y. Choi, and B. H. Hong, Nature (London) **457**, 706 (2009).

[12] Y. Pan, H. Zhang, D. Shi, J. Sun, S. Du, F. Liu, and H. Gao, Adv. Mater. **21**, 2777 (2009).

[13] J. Witterlin and M.-L. Bocquet, Surf. Sci. **603**, 1841 (2009).

[14] Z. H. Ni, W. Chen, X. F. Fan, J. L. Kuo, T. Yu, A. T. S. Wee, and Z. X. Shen, Phys. Rev. B **77**, 115416 (2008).

[15] G. Rogers and J. Z. Liu, J. Am. Chem. Soc. **133**, 10858 (2011).

[16] C. Lee, X. Wei, J. W. Kysar, and J. Hone, Science **321**, 385 (2008).

[17] S. Joseph and N. R. Aluru, Nano Lett. **8**, 452 (2008).

[18] S. Bernardi, B. D. Todd, and D. J. Searles, J. Chem. Phys. **132**, 244706 (2010).

[19] S. Plimpton, J. Comput. Phys. **117**, 1 (1995).

[20] H. Berendsen, J. R. Grigera, and T. P. Straatsma, J. Phys. Chem. **91**, 6269 (1987).

[21] J. P. Ryckaert, G. Ciccotti, and H. Berendsen, J. Comput. Phys. **23**, 327 (1977).

[22] T. Werder, J. H. Walther, R. L. Jaffe, T. Halicioglu, and P. Koumoutsakos, J. Phys. Chem. B **107**, 1345 (2003).

[23] R. W. Hockney and J. W. Eastwood, *Computer simulation using particles* (Institute of Physics Publishing, Bristol [England], Philadelphia, 1992).

[24] M. D. Ma, L. Shen, J. Sheridan, J. Z. Liu, C. Chen, and Q. Zheng, Phys. Rev. E **83**, 36316 (2011).

[25] F. Yang, Chem. Eng. Commun. **197**, 544 (2010).

[26] L. Bocquet and J. L. Barrat, Soft Matter **3**, 685 (2007).

[27] K. Falk, F. Sedlmeier, L. Joly, R. R. Netz, and L. Bocquet, Nano Lett. **10**, 4067 (2010).

[28] P. E. Smith and W. F. van Gunsteren, Chem. Phys. Lett. **215**, 315 (1993).

[29] J. A. Thomas and A. McGaughey, Nano Lett. **8**, 2788 (2008).

[30] R. S. Voronov, D. V. Papavassiliou, and L. L. Lee, Ind. Eng. Chem. Res. **47**, 2455 (2008).

[31] X. Qin, Q. Yuan, Y. Zhao, S. Xie, and Z. Liu, Nano Lett. **11**, 2173 (2011).

[32] M. P. Allen and D. J. Tildesley, *Computer Simulation of Liquids* (Oxford University Press, New York, 1989).

[33] L. Bocquet and J. L. Barrat, Phys. Rev. E **49**, 3079 (1994).

[34] P. Espanol and I. Zuniga, J. Chem. Phys. **98**, 574 (1993).

[35] A. N. Lagar'kov and V. M. Sergeev, Sov. Phys. Usp. **21**, 566 (1978).

[36] J. Petravic and P. Harrowell, J. Chem. Phys. **127**, 174706 (2007).

[37] J. S. Hansen, B. D. Todd, and P. J. Daivis, Phys. Rev. E **84**, 016313 (2011).

[38] F. Guinea, M. I. Katsnelson, and A. K. Geim, Nat. Phys. **6**, 30 (2010).

[39] S.-M. Choi, S.-H. Jhi, and Y.-W. Son, Phys. Rev. B **81**, 081407(R) (2010).

[40] S. Grimme, J. Comput. Chem. **27**, 1787 (2006).

[41] J. Ma, A. Michaelides, D. Alfè, L. Schimka, G. Kresse, and E. Wang, Phys. Rev. B **84**, 033402 (2011).

[42] D. Mattia and Y. Gogotsi, Microfluid. Nanofluid. **5**, 289 (2008)

[43] S. Ghosh, A. K. Sood, and N. Kumar, Science **299**, 1042 (2003).

[44] P. Dhiman, F. Yavari, X. Mi, H. Gullapalli, Y. Shi, P. M. Ajayan, and N. Koratkar, Nano Lett. **11**, 3123 (2011).